Robotica: (2019) volume 37, pp. 1641–1662. © Cambridge University Press 2019
doi:10.1017/S0263574719000171

Multi-DoFs Exoskeleton-Based Bilateral Teleoperation with the Time-Domain Passivity Approach

Domenico Buongiorno*, Domenico Chiaradia, Simone Marcheschi, Massimiliano Solazzi and Antonio Frisoli

PERCRO Laboratory, TeCIP Institute, Scuola Superiore Sant'Anna, Pisa, Italy.
E-mails: domenico.chiaradia@santannapisa.it, simone.marcheschi@santannapisa.it, massimiliano.solazzi@santannapisa.it, antonio.frisoli@santannapisa.it

(Accepted January 19, 2019. First published online: March 1, 2019)

SUMMARY
It is well known that the sense of presence in a tele-robot system for both home-based tele-rehabilitation and rescue operations is enhanced by haptic feedback. Beyond several advantages, in the presence of communication delay haptic feedback can lead to an unstable teleoperation system. During the last decades, several control techniques have been proposed to ensure a good trade-off between transparency and stability in bilateral teleoperation systems under time delays. These proposed control approaches have been extensively tested with teleoperation systems based on identical master and slave robots having few degrees of freedom (DoF). However, a small number of DoFs cannot ensure both an effective restoration of the multi-joint coordination in tele-rehabilitation and an adequate dexterity during manipulation tasks in rescue scenario. Thus, a deep understanding of the applicability of such control techniques on a real bilateral teleoperation setup is needed. In this work, we investigated the behavior of the time-domain passivity approach (TDPA) applied on an asymmetrical teleoperator system composed by a 5-DoFs impedance designed upper-limb exoskeleton and a 4-DoFs admittance designed anthropomorphic robot. The conceived teleoperation architecture is based on a velocity–force (measured) architecture with position drift compensation and has been tested with a representative set of tasks under communication delay (80 ms round-trip). The results have shown that the TDPA is suitable for a multi-DoFs asymmetrical setup composed by two isomorphic haptic interfaces characterized by different mechanical features. The stability of the teleoperator has been proved during several (1) high-force contacts against stiff wall that involve more Cartesian axes simultaneously, (2) continuous contacts with a stiff edge tests, (3) heavy-load handling tests while following a predefined path and (4) high-force contacts against stiff wall while handling a load. The found results demonstrated that the TDPA could be used in several teleoperation scenarios like home-based tele-rehabilitation and rescue operations.

KEYWORDS: Multi-DoFs asymmetrical teleoperation; TDPA; Exoskeleton; Passivity; Tele-rehabilitation; Disaster scenario.

1. Introduction

Robots are becoming more and more ubiquitous and are contributing in overcoming human limits in fields such as industry, medicine, rehabilitation[1–5] and assistance.[6–9] One powerful feature of robotic systems is the possibility to teleoperate them by a remote station. Teleoperation is spreading out in

* Corresponding author. E-mail: domenico.buongiorno@santannapisa.it

home-based rehabilitative systems where the use of robotic technology has been demonstrated to be useful in overcoming the challenges of a successful home rehabilitation and to meet the needs of all the patients involved.[10,11] A more challenging scenario for robotic teleoperation systems is the search and rescue in environments affected by natural catastrophes as earthquake or human-made disasters, as in the case of a nuclear accident. Disaster scenarios, like the Fukushima nuclear accident, have clearly shown the limits of today disaster-response robots for providing support to rescue operations. Tele-robotics is one of the most successful and versatile technologies in disaster response.[12–14] Real-time teleoperation is an appealing technology in these scenarios as it combines robotic capabilities with human intelligence and manipulation skills, and haptic feedback is the solution that can enhance the sense of presence of the operator that acts remotely at the disaster place through the slave robot.

In this context, this paper presents a part of the work done in the framework of the European H2020 project CENTAURO (https://www.centauro-project.eu) that has the aim to develop a robot-based disaster-response system. It consists of a Centauro-like robot (with four legs and two arms), operator interfaces including a full-body tele-presence suite (based on two fully 7 degrees of freedoms (DoF) actuated exoskeleton arms), autonomous locomotion and manipulation functions, and modules for communication and simulation.

A crucial aspect we had taken into account is the quality of the communication connection between the master operator and the remote robot. In fact, it is well known that communication delays in bilateral teleoperation can lead to an unstable behavior of the teleoperator system. Teleoperation is said to be *bilateral*[15] if the slave has force sensors that can reflect back to the master the interaction forces with the environment while the human imposes a force on the master which in turn results in a movement that is transmitted to the slave for replying it.

From a theoretical point of view, a bilateral teleoperator system should achieve the following two goals at the same time: (i) *transparency*: that is, the ability of the robotic system to render the mechanical property of the remote environment without introducing distortions and (ii) *stability*: that is, to keep closed-loop system stable irrespective of the behavior of the operator or the environment. Stability and transparency of the teleoperation system are two competing objectives, between which a trade-off has to be achieved. Hence, the trade-off is the minimum level of transparency necessary for efficient task execution without making the system unstable.[15] The modeling and control of the teleoperation in such systems still present a challenge due to instability introduced by the communication affected by randomly varying delays, discrete-time exchange of data and loss of information.[16] Several control techniques have been proposed to overcome the above-mentioned problems:[17] passivity-based approaches[18,19] (wave variables, time-domain passivity approach—TDPA, adaptive controllers), four-channel architecture,[20] sliding-mode control,[21] H_∞ design,[22] and model-mediated control.[23]

In the last decades, research groups mainly focused on the development of sophisticated robotic devices conceived to act remotely that can be used as *slave robots*[24–26] or to be worn by a subject to control the remote slave robot (that can be used as *master robot*, i.e., exoskeletons).[26,27] The design process of both families of robots tends to consider an increasing number of DoFs leading to high-level manipulation skills. However, since several theoretical control approaches have been proposed and tested only in simulation or with simple 1-DoF robotic/haptic interfaces, there is a lack of experimental studies that investigate and evaluate the use of such control techniques with advanced multi-DoF robotic platforms in realistic scenarios. Few presented works investigated how teleoperation control approaches can be used in real scenarios, but they are limited to desktop haptic devices or joysticks with few DoFs.[28,29] Compared to simple desktop haptic devices and joysticks, multi-DoFs exoskeletons allow for a dexterous control of the full pose of the remote robotic arm. Some studies have presented a complex robotic teleoperation platform including a bimanual upper-limb exoskeleton,[26] but with the limitation that the communication time delay is not considered.

TDPA is one of the most used approach. The majority of the published papers on TDPA discusses the application of the technique to teleoperator systems based on two equal master and slave with few DoFs,[17,30–33] most of them only 1 DoF. Hence, the study of the TDPA has not been deeply extended to more complex teleoperator systems yet. As an example, it is not clear what would be the TDPA effect if the master and slave were mechanically completely different. In particular, we are interested in analyzing the TDPA with an asymmetrical multiple DoFs teleoperator system with master and slave characterized by opposite mechanical performances: admittance type and impedance type.

https://doi.org/10.1017/S0263574719000171 Published online by Cambridge University Press

Fig. 1. Master device: the arm light exoskeleton (ALEx).

In this study, the authors investigated and evaluated the application of the TDPA to a complex teleoperation setup composed of two multi-DoFs robotic devices under time-delayed communication. The chosen setup is asymmetrical since the two robotics are different from both the mechanic and kinematic point of view. Extending the TDPA to an asymmetrical multi-DoFs teleoperation setup, the authors evaluated a large set of experimental trials in teleoperation including stiff wall collisions (against both a simple wall and a corner), stiff surface following, load handling and contacts while handling a load. From the experiments emerged a limitation of some aspects of TDPA, that have been overcome proposing of a new solutions.

The paper is organized as follows. Section 2 describes the experimental setup based on two different robotic devices and the designed and adopted bilateral teleoperation control architecture including the proposed energy resetting heuristic. The experiments and the results are reported in Sections 3 and 4, respectively, and are discussed in Section 5. Finally, Section 6 concludes the paper.

2. Materials and Methods

This section introduces the physical setup and the control architecture adopted for this work. Section 2.1 briefly describes the master and the slave robots and their unilateral control strategies, whereas Section 2.2 mentions the position–force time-domain passivity theory and a control strategy to compensate for slave position drifting. In order to overcame problems related to energy accumulation of the passivity observer (PO), a novel energy resetting heuristic has been introduced. Finally, this section explains the method we had used to take into account for different kinematics of the two exoskeletons.

2.1. Teleoperation system

The teleoperation system involved two robotic devices previously developed at the PERCRO laboratory. The master device is the arm light exoskeleton (ALEx) (see Fig. 1) that is a 4-DoFs (+1 not actuated) impedance-like upper-limb exoskeleton.[34] In this work, we used the latest version of ALEx featuring two arms, but only the left-arm has been used for the bilateral teleoperation experiments. The slave robot is the Rehab-Exos (see Fig. 2) that is 4-DoFs admittance-like exoskeleton.[35,36] The chosen setup is asymmetrical since the two robotics are different from both the mechanic and kinematic point of view.

2.1.1. Master device. ALEx is composed of two mechanically compliant robotic arms designed for the human upper limbs. The work by Pirondini et al.[34] illustrates the description of ALEx previous version, developed to support only the right arm. Besides the introduction of the left arm, the current version of the device features the following novelties:

- high dynamic performance brushless motors, selected for further reduction of the inertia experienced by the patient;
- more robust and reliable routing of the mechanical cable transmission;

https://doi.org/10.1017/S0263574719000171 Published online by Cambridge University Press

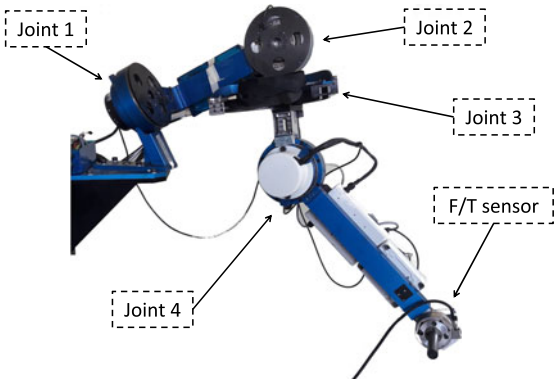

Fig. 2. Slave device: the Rehab-Exos exoskeleton.

- robotic arms and seat equipped with motorized slides to adjust the users position in the front/horizontal and vertical direction.

Its workspace is approximately 90% of that of the human arm. The *ALEx* has four actuated DoFs for supporting elbow and shoulder movements: shoulder adduction/abduction, shoulder flexion/extension, shoulder internal/external rotation, elbow flexion/extension—and one passive DoF used for measuring the wrist prono-supination angle. The ALEx is able to generate a maximum continuous force at the end-effector (EE) equal to 50 N and a peak force of 100 N in the worst case. In a central position of the workspace, the bandwidth and stiffness at the EE level are 10 Hz and 1000 N/m, respectively.

Since in a teleoperation application the master device is used to render force feedback, the ALEx exoskeleton joints are controlled using the following law:

$$\boldsymbol{\tau}_J = \boldsymbol{\tau}_J^G + \boldsymbol{\tau}_J^{VF} + J^T \boldsymbol{F}_{\boldsymbol{EE}} \tag{1}$$

where $\boldsymbol{\tau}_J$ is the vector of the joint control torques, $\boldsymbol{\tau}_J^G$ is the feed-forward gravity compensation term, $\boldsymbol{\tau}_J^{VF}$ is the feed-forward viscous friction compensation term, $\boldsymbol{F}_{\boldsymbol{EE}}$ is the renderized spatial force at the EE, and J^T the transposed Jacobian.

2.1.2. Slave device. The Rehab-Exos is an active robotic exoskeleton (Fig. 2) conceived for rehabilitation applications, and also, due to its mechanical characteristics, it is suitable for power augmentation. It has an admittance-type robot construction with joint motor groups characterized by embedded torque sensor and high ratio gear reduction.

It is designed to generate controlled contact forces/torques not only at its end-link handle, but also at intermediate links. For this research study, it has been used as a position controlled manipulator to apply forces with the EE.

As depicted in Fig. 2, the Rehab-Exos has a serial architecture isomorphic with the human kinematics that comprises: a shoulder joint fixed in space and composed by three active joints J_1, J_2, and J_3 and an active elbow joint J_4. For a more detailed description of both Rehab-Exos and actuation groups the reader can refer to work published by Vertechy et al.[35] The three joints J_1, J_2, and J_4 of the exoskeleton are motorized through identical actuation groups. Each joint features a custom-made frame-less brush-less torque motor integrating a compact Harmonic Drive (HD) component set. The actuator provides a joint output torque equal to 150 Nm with an overall weight equal to 3.7 kg and a motor shaft inertia reduced to the joint output shaft $J_m = 3.7$ kg·m^2. The maximum force the robot can exert at the EE in the worst case is 150 N in any direction. Moreover, the HD performs a reduction equal to 100:1, thus the joints feature limited back-drivability at motor power-off. Joint J_3 is characterized by a tendon transmission that is used to transmit the actuation torque through an open semi-circular guide.

The three joints J_1, J_2, and J_4 have a torque sensor which is located at the joint output shaft. The internal joint-torque sensor introduces controlled torsional compliance that is used at the same time to transmit joint-torque actuation from the motor to the link and to measure it. In a central position of the workspace, the bandwidth and stiffness at the EE level are 20 Hz and 40,000 N/m, respectively.

https://doi.org/10.1017/S0263574719000171 Published online by Cambridge University Press

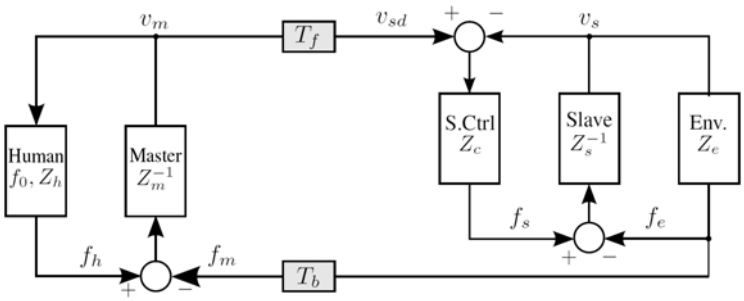

Fig. 3. The block diagram of the P–F (measured) teleoperation architecture. Contribution from the work of Artigas et al.[40]

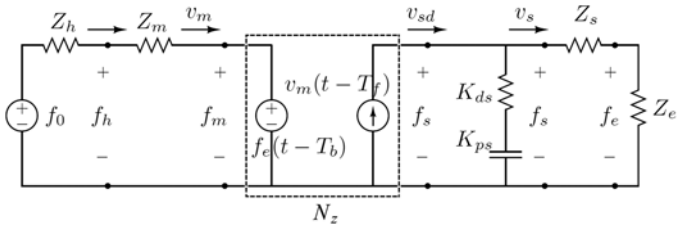

Fig. 4. Equivalent electrical scheme of the P–F measured architecture. Contribution from the work of Artigas et al.[40]

Since in a teleoperation application the slave device is used to execute the position tracking task in the Cartesian space, the slave joints are controlled using the following law:

$$\boldsymbol{\tau}_J = \boldsymbol{\tau}^{\mathbf{dyn}} + \boldsymbol{\tau}_J^G + K_P(\boldsymbol{q}^* - \boldsymbol{q}) - K_D(\dot{\boldsymbol{q}}^* - \dot{\boldsymbol{q}}) \tag{2}$$

where $\boldsymbol{\tau}_J$ is the vector of the joint control torques, $\boldsymbol{\tau}^{\mathbf{dyn}}$ are the dynamic compensation terms, and $\boldsymbol{\tau}_J^G$ is the feed-forward gravity compensation term (for the dynamic compensations, please refer to work proposed by Solazzi et al.[36]). $\boldsymbol{q}^*$ and $\boldsymbol{q}$ are the vector of the desired and actual joint positions, respectively; K_P and K_D are the proportional and derivative constants of the PD position controller, respectively.

2.2. Bilateral teleoperation control

2.2.1. Time-domain passivity control for position–force (measured) architecture. The choice of TDPA technique is motivated by its main advantage, that is, it is model-insensitive (or model-free), then it can accommodate a large class of systems since its performance depends only on measurements. TDPA was first introduced by Hannaford et al. as method for controlling a haptic interface system to ensure stable contact with a virtual wall.[37] After few years, the same method was extended to apply to teleoperation systems.[38] The TDPA consists of monitoring the energy of the system in real-time (by using POs) and dissipating it only when the system presents an active behavior (by using passivity controllers—PCs).The TDPA[37,38] has been tested in many conditions: with and without time-delay, with fixed or varying time-delay, with data loss and communication stop events. The TDPA has been introduced in several bilateral teleoperation schemas: position–position, position–control force, position–measured force. In this study, we chose the position–measured force (P–F_{meas}) architecture due to its ability to ensure a high level of transparency in free motion.[39] As depicted in the (P–F_{meas}) schema (Fig. 3), the velocity (or position) command sent to the slave robot, v_{sd}, is the master velocity, v_m delayed; and the slave force signal, f_e, is fed back to the master device.[40]

A more useful schema can be derived from the block diagram (Fig. 4) using electrical circuit theory (Fig. 4). It derives that the signal pairs describing each port of the communication are as follows:

- *Master side* : $f_m(t) = f_e(t - T_b)$ and $v_m(t)$,
- *Slave side* : $f_s(t)$ and $v_{sd} = v_m(t - T_f)$,

https://doi.org/10.1017/S0263574719000171 Published online by Cambridge University Press

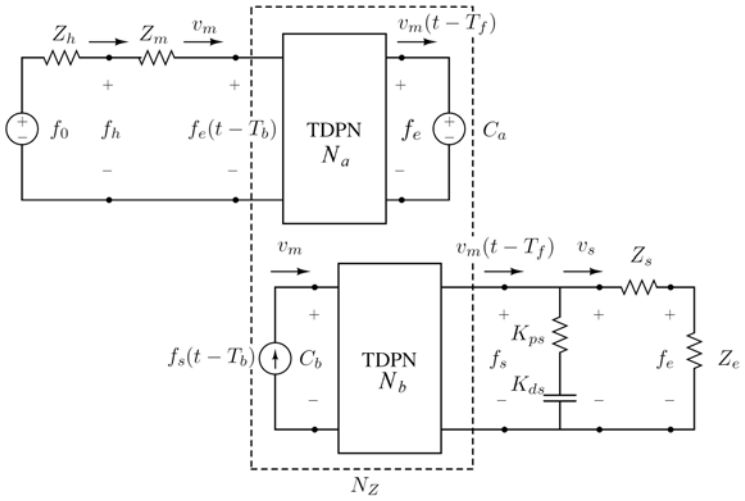

Fig. 5. The network N_Z can be segmented within two dependent ideal sources, C_a and C_b, and two time delay power networks, N_a and N_b. Contribution from the work of Artigas et al.[40]

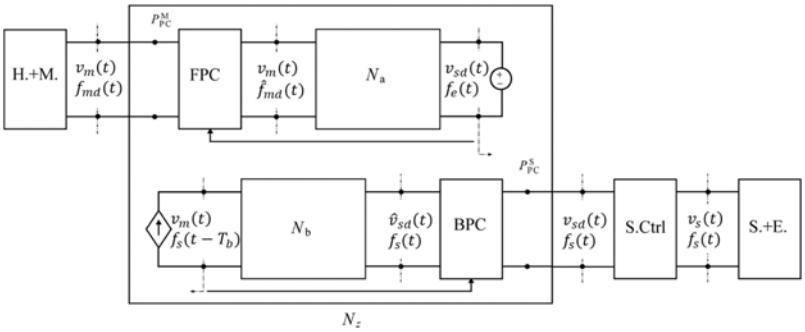

Fig. 6. The passivation of the two networks N_a and N_b achieved with the forward and backward passivity controllers (FPC-BPC), where $\hat{v}_{\mathrm{sd}}(t) = v_m(t - T_f)$ and $\hat{f}_{\mathrm{md}}(t) = f_e(t - T_b)$. Contribution from the work of Artigas et al.[40]

where f_m is the force that has to be rendered by the master, f_s is the actuation force of the slave, and T_f and T_b are the forward and backward communication delays, respectively.

In order to apply the TDPA theory to the schema shown in Fig. 4, some equivalent representation changes are needed. The network N_Z, containing two ideal sources (Fig. 4), can be represented combining two undelayed dependent sources and two time-delay power networks (TDPNs) carrying the energy of each undelayed dependent source (Fig. 5).[40] It is worth noting that the augmented network N_Z carries the energy due to the delay and the sources C_a and C_b. This can be seen as follows:

$$\begin{aligned} E_{N_z}(t) &= \int_0^t \left[f_e(\tau - T_b)\, v_m(\tau) - f_s(\tau) v_m\left(\tau - T_f\right) \right] d\tau \\ &= E_{N_a}(t) + E_{C_a}(t) + E_{N_b}(t) + E_{C_b}(t) \end{aligned} \tag{3}$$

where $E_{N_a}(t)$ and $E_{N_b}(t)$ are the energy flows of N_a and N_b; and E_{C_a} and E_{C_b} are the energy flows of the sources attached to N_a and N_b, respectively ($E_{N_a}(t)$, $E_{N_b}(t)$, E_{C_a} and E_{C_b} definitions can be found in the Appendix).

The channel passivity is then ensured by the observation and passivation of $E_{N_a}(t)$ and $E_{N_b}(t)$. It is worth noting that in the ideal condition, $T_f = T_b = 0$, both $E_{N_a}(t)$ and $E_{N_b}(t)$ become null. As mentioned earlier, the TDPA has two main components: a PO which monitors the energy flow of the network and a PC which dissipates the energy introduced by the active elements in the network. Regarding the P–F measured architecture, the TDPA models and makes passive the bilateral teleoperation system using two TDPNs and two POs/PCs (Fig. 6), that is, a forward PC, or FPC, and a backward PC, or BPC.

https://doi.org/10.1017/S0263574719000171 Published online by Cambridge University Press

Passivity observers and controllers: POs are real-time computation of the passivity conditions, taking into account the energy dissipated by the PCs. The two POs, $W_S(n)$ for the slave and $W_M(n)$ for the master, have been defined as in the study proposed by Artigas et al.[40] and can be found in the Appendix.

The PCs are variable dampers which bound the output energy of a port by the input energy from the opposite port by dissipating any extra energy. The equations of the PC are as follows. The FPC takes the following form for each component:

$$f_{\mathrm{md}}(n) = \hat{f}_{\mathrm{md}}(n) + \alpha(n) v_m(n) \tag{4}$$

where $\hat{f}_{\mathrm{md}}(n) = f_e(n - T_{kb})$ is the untouched force signal coming from the slave. The coefficient $\alpha(n)$ is given as follows:

$$\alpha(n) = \begin{cases} 0, & \text{if } W_M(n) > 0 \\ \dfrac{-W_M(n)}{\Delta T v_m^2(n)}, & \text{else if } |v_m(n)| > 0 \end{cases} \tag{5}$$

and the energy dissipated by the FPC is given for each component as

$$E_{FPC}^M(n) = \Delta T \sum_{n=0}^{n=k} \alpha(n) v_m^2(n) \tag{6}$$

At the slave side, BPC takes the form:

$$v_{\mathrm{sd}}(n) = \hat{v}_{\mathrm{sd}}(n) - \beta(n) f_s(n) \tag{7}$$

for each x, y, z component indicated here with i index, where $\hat{v}_{\mathrm{sd}}(n) = v_m(n - T_{kf})$ is the untouched velocity signal from the master. The coefficient $\beta(n)$ is given as follows:

$$\beta(n) = \begin{cases} 0, & \text{if } W_S(n) > 0 \\ \dfrac{-W_S(n)}{\Delta T f_s^2(n)}, & \text{else if } |f_s(n)| > 0 \end{cases} \tag{8}$$

and the energy dissipated by the BPC is given as follows:

$$E_{\mathrm{BPC}}^S(n) = \Delta T \sum_{n=0}^{n=k} \beta(n) f_s^2(n) \tag{9}$$

2.2.2. Slave position drift compensation.

Cause of position drift: Ideally, the slave controller should ensure that the slave position follows the delayed mater position. However, since position and force signals are not power correlated, the master sends the velocity signal over the communication channel. Then, the slave controller obtains the position reference $p_{\mathrm{sd}}(n)$ by integrating the velocity $v_{\mathrm{sd}}(n)$.

The BPC modifies the received master velocity $\hat{v}_{\mathrm{sd}}(n)$ to dissipate energy as given by (7). Thus, the modified position command signal for the slave controller incurs drift given as

$$p_{\mathrm{err}}(n) = \Delta T \sum_{n=0}^{n=k} \left[v_{\mathrm{sd}}(n) - \hat{v}_{\mathrm{sd}}(n) \right] = \Delta T \sum_{n=0}^{n=k} \beta(n) f_s(n) \tag{10}$$

Thus, position drift is accumulated whenever slave PC is active ($\beta(n) \neq 0$ and $f_s(n) \neq 0$).

Position drift compensation—energy injection: In 2014, Chawda et al. proposed a method to inject energy at the slave side that counters the position drift during the instants when the channel is passive.[32] The proposed scheme is shown in Fig. 7. The energy injected is always bound by the slave side PO/PC, hence ensuring system passivity. So in proposed scheme, the variable value of the dependent flow source $v_{\mathrm{ad}}(n)$ is set as follows:

https://doi.org/10.1017/S0263574719000171 Published online by Cambridge University Press

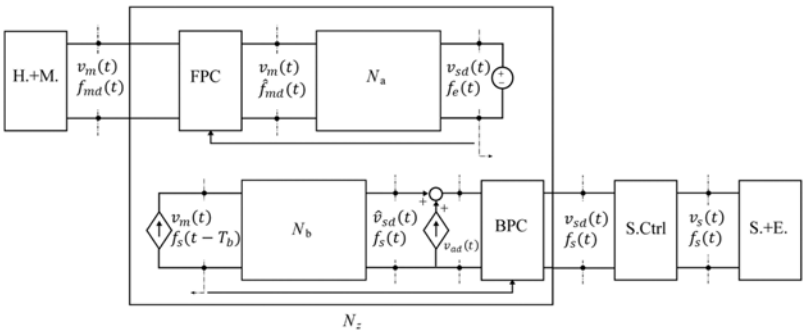

Fig. 7. Energy injection via a dependent flow source to compensate for the position drift. Slave PO/PC passivates both the TDPN and the additional flow source.

$$v_{\mathrm{ad}}(n) = \frac{1}{\Delta T}\left[\hat{p}_{sd}(n) - \Delta T \sum_{k=0}^{k=n-1} v_{\mathrm{sd}}(k) - \hat{v}_{\mathrm{sd}}(n)\Delta T\right] \tag{11}$$

2.2.3. Energy resetting heuristic. One of the main problems associated with the TDPA is the accumulation of energy dissipation. As an example, consider an environment characterized by a dissipative area and an active area. If the user spent a lot of time interacting with the dissipative area the PO may build up a large amount of positive of energy, that is, $W_{M/S}(n)$ would have a large positive value. Then, if the user starts to interact with the active area (the value of $W_{M/S}(n)$ would start decreasing), the PC will not intervene until the active behavior is observed, that is, $W_{M/S}(n) < 0$. This explains the need for an energy resetting procedure that have to set the value of $W_{M/S}(n)$ to zero. The method proposed by Kim and Hannaford considers a PO that is reset when the absolute value of the rendered force is less than a certain threshold for a fixed amount of time,[41] in other words when the salve is not interacting with the environment. Some years later Ryu proposed an energy resetting scheme that resets the PO if there is no active energy output, that is, the system is stable, for certain amount of time.[42]

In this paper, we proposed a mixed approach that is based on both methods reported above. In particular, the PO on the master side is reset if $|f_e(k - T_b)| < \epsilon$ *AND* $W_M(n) > 0$ for τ seconds, whereas the slave PO is reset if $|f_e(k)| < \epsilon$ *AND* $W_S(n) > 0$ for τ seconds. This new proposed heuristic ensures that a PO is reset only if there is no interaction between the slave and the environment, and the teleoperator system is stable. This may prevent that the POs are reset either during a contact, as it could happen using the Kim's approach, or during a unstable free movement, as it could happen using the Ryu's technique.

2.2.4. Bilateral teleoperation control. Since the remote manipulation tasks are defined in the Cartesian space, master and slave share the information regarding the three translational DoFs at the EE level: Positions, Velocities, and Forces. For this reason, the TDPA theory has been implemented for each of the 3 DoFs, independently.

It is worth noting that the master imposes an EE position to the slave, but the slave has 4 DoFs. Although master and slave share some kinematic characteristics (serial kinematic with four revolute joints), at the same time the two robots have different link lengths, then different workspaces (the two robots can be shown in Fig. 9). In order to solve the slave redundancy, the slave pose was set by using an inverse kinematic algorithm (Fig. 8) able to minimize the difference between the pose of the master and the slave. In detail, the slave position target is updated by integrating the sent master velocities (see (12)).

$$\boldsymbol{p_{sd}}(k) = \sum_{k=1}^{K} \boldsymbol{V_{sd}}(k) + \boldsymbol{p_{sd}}(0) \tag{12}$$

where $\boldsymbol{p_{sd}}(k)$ is the slave target position at time k, which is calculated using the master velocities received from the starting time to the time k. The related formulas of the schema in Fig. 8 are (13) and (14) where q_s^i is the ith slave joint angle, q_m^i is the ith master joint angle, n is the number of slave joints and J and $J^\dagger$ the Jacobian and the Jacobian pseudoinverse of the slave, respectively,

https://doi.org/10.1017/S0263574719000171 Published online by Cambridge University Press

Table I. The proportional and derivative gains used for the four joint slave position controls.

Joint	K_p **[N·m/rad]**	K_d **[N·m·s/rad]**
J1	4000	40
J2	3000	40
J3	3000	50
J4	5000	35

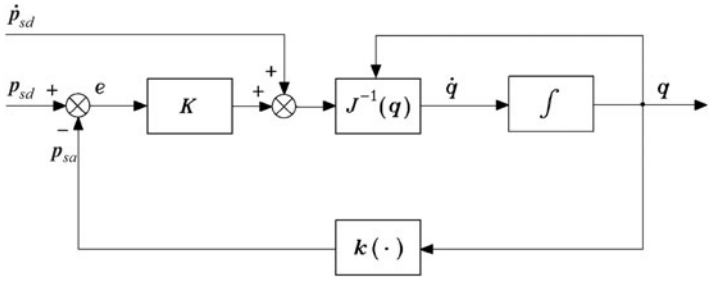

Fig. 8. Inverse kinematics scheme without optimization component. Contribution from the book of Sciavicco and Siciliano.[43]

$$\dot{\boldsymbol{q}} = J^{\dagger}(\dot{\boldsymbol{p}}_{\boldsymbol{sd}} + K\boldsymbol{e}) + (I_n - J^{\dagger}J)\dot{\boldsymbol{q}}_{\boldsymbol{0}} \tag{13}$$

$$\dot{\boldsymbol{q}}_{\boldsymbol{0}} = K_0 \left(\frac{\partial w(q)}{\partial \boldsymbol{q}}\right)^T \quad \boldsymbol{w(q)} = -\frac{1}{2n}\sum_n^{i=1}(\boldsymbol{q}_{\boldsymbol{s}}^{\boldsymbol{i}} - \boldsymbol{q}_{\boldsymbol{m}}^{\boldsymbol{i}})^2 \tag{14}$$

The solution solves the redundancy inverse kinematic problem by minimizing the function $w(q)$, minimizing distance from the angular limits, through the computation of its gradient in (14).

3. Experiments

To evaluate the performance of the position–force (measured) TDPA schema with a realistic asymmetrical multi-DoF setup, we used two mechanically different robots in a benchmark composed by four main set of experiments. In a real scenario, the user that drives the master needs a device as much lightweight and transparent as possible featuring by an high fidelity haptic rendering. The slave robot has to exhibit a solid structure, the possibility to carry a weight up to 10 kg and an high dynamic bandwidth.

Regarding the master device, the local control is an open-loop force control. In detail, the master controller applies to the master device: (1) the torques/forces to be rendered (obtained from the slave measured forces), (2) the gravity compensation torques, and (3) both the static and viscous friction compensation terms to ensure the transparency. The slave device implements a closed-loop position control, that is, a PD control with a gravity and dynamic compensation. Dynamic compensation term is computed by using an acceleration observer that use both joint-torque sensors and encoder position reads. The proportional and derivative gains of the slave position control have been chosen such that the position error at the EE (when no forces are applied at the EE) is less than 0.5 mm with a maximum speed of 0.5 m/s. The gains used in these experiments are reported in Table I.

Both the master and slave controller ran with a time step of 200 μs, while the round-trip communication delay was less than 1 ms when no time delay was introduced. All the conducted experiments involved the master robot's left arm because the slave exoskeleton was configured as a left arm. The proposed benchmark is composed by the following four set of experiments:

- (Exp-1) Brief and impulsive contact with flat stiff surfaces;
- (Exp-2) Continuous contact with a stiff nonplanar surface;
- (Exp-3) Trajectory following with a constant load at slave EE;
- (Exp-4) Brief and impulsive contact with flat stiff surfaces while handling a load.

https://doi.org/10.1017/S0263574719000171 Published online by Cambridge University Press

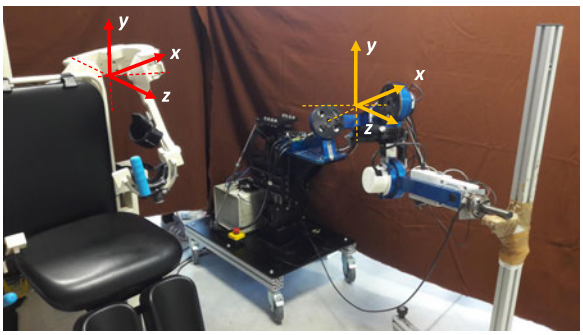

Fig. 9. The setup of the experiment Exp-1 with the reference systems of the two robots. Left: the master device without the human operator. Centre: the slave device. Right: a physical contact with a rigid environment.

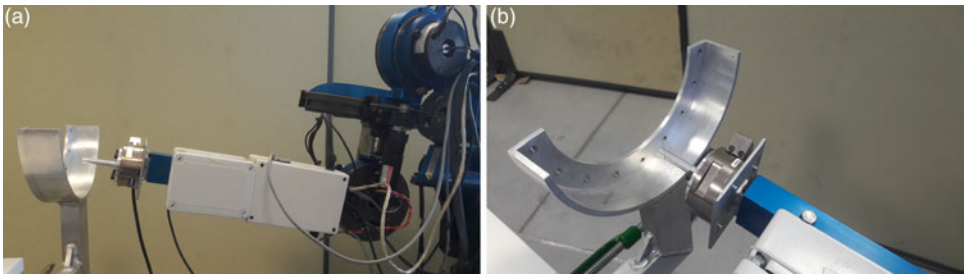

Fig. 10. The setup of the experiment Exp-2. (a) The exoskeleton arm while approaching the round stiff surface. (b) A particular of the aluminum round-shaped stiff surface.

3.1. Experiment—Exp-1

For the experiment Exp-1, the setup was composed of the two robotic devices and a solid structure used to perform high-stiffness contacts along three surfaces, one for each Cartesian axis. A picture of the system setup for the experiment Exp-1 is shown in Fig. 9.

The bilateral teleoperation system was initially tested without communication delay, both in free movement and in contact with the rigid environment, i.e., the rigid solid body. In these two conditions the overall system exhibited a stable behavior without the necessity of the PC. Then, to evaluate the TDPA in a real teleoperation, an high time delay was introduced. The simulated communication delay was set to 40 ms in both directions (from and to the master device), that is, 80 ms round-trip. The experiment Exp-1 was then articulated in three different tests:

- contact with flat surfaces in the three Cartesian axes (each individually), with delay and the PC on;
- contact with flat surfaces in the three Cartesian axes (each individually), with delay and the PC off;
- contact with a sharp corner (two or three Cartesian axes involved), with delay and the PC on.

In all the tests the user was asked to drive the slave robot closed to the stiff surface and try to push the slave EE against it as long as possible.

3.2. Experiment—Exp-2

In the experiment Exp-2 the master exoskeleton's driver was asked to teleoperate the slave robot while keeping a continuous contact with a stiff non-planar surface (Fig. 10). The selected surface was a semi-circumference of an aluminum piece with a radius of 90 mm. This experiment has the objective to evaluate the control performance in the scenario of a continuous force exchange between the slave and the environment as for example in a door opening task or in a valve turning task. The experiment Exp-2 was articulated in two different tests:

- continuous contact in case of delay and PC on;
- continuous contact in case of delay and PC off.

https://doi.org/10.1017/S0263574719000171 Published online by Cambridge University Press

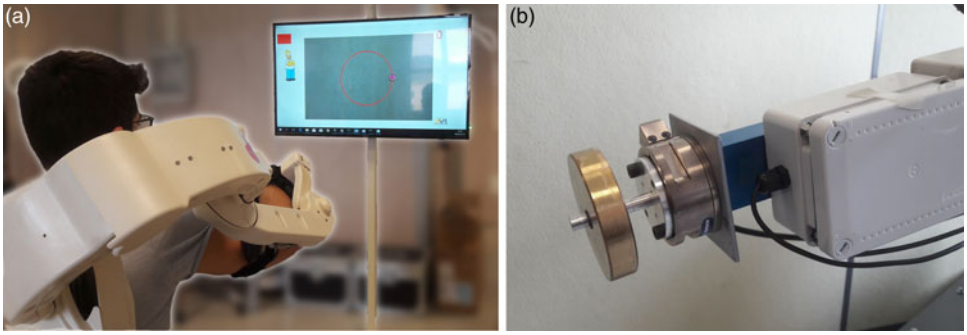

Fig. 11. The setup of the experiment Exp-3. (a) The master exoskeleton worn by the driver while performing the trajectories at constant speed. The positions' reference are given through a visual target displayed on a screen. (b) A particular of the slave's EE where the external mass was mounted.

Fig. 12. The setup of the experiment Exp-4. A 1-kg cylindrical load is attached at the slave EE. The driver of the master exoskeleton was asked to handle the load and perform several contacts against a stiff surface.

3.3. Experiment—Exp-3

The experiment Exp-3 consisted in a load handling in the workspace. The master exoskeleton's user was asked to follow a visual circular reference trajectory (diameter was equal to 260 mm) at a constant angular speed of 0.7 rad/s. A 1 kg cylindric load was attached at the EE handle of the slave robot. The setup of the experiment Exp-3 is depicted in Fig. 11.

Also the experiment Exp-3 was articulated in two different tests: that is, in case of delay and PC on and in case of delay and PC off.

3.4. Experiment—Exp-4

During the experiment Exp-4, the driver of the master was asked to perform contacts against a stiff surface while handling a load that was a 1 kg cylindric mass. The setup of the experiment Exp-4 is depicted in Fig. 12.

As the previous experiments, also the experiment Exp-4 was articulated in two different tests: i.e., in case of delay and PC on and in case of delay and PC off.

4. Results

This section reports the results of the set of experiments described above.

https://doi.org/10.1017/S0263574719000171 Published online by Cambridge University Press

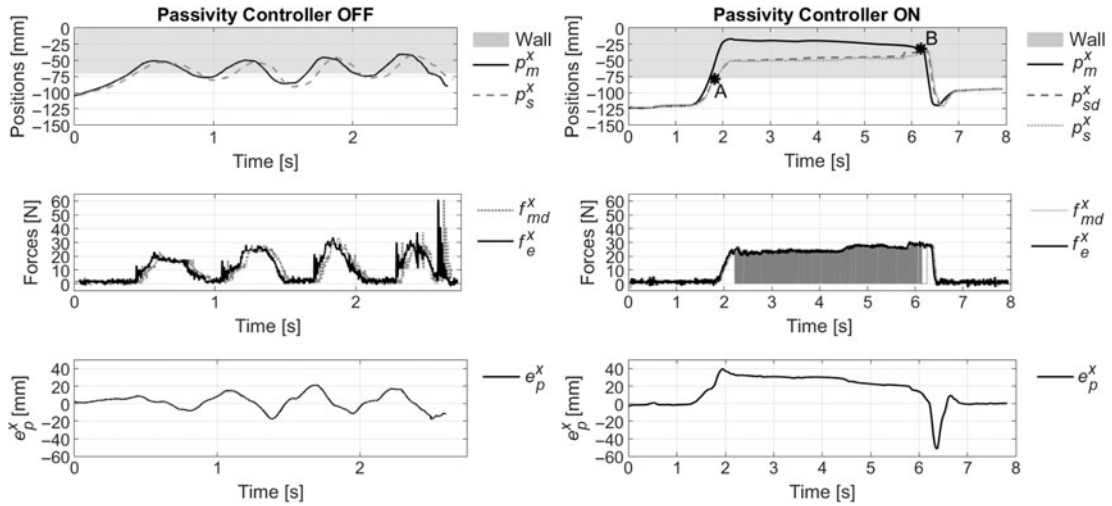

Fig. 13. Comparison between a stable and an unstable contact along the *X*-axis. Left: the experiments without the passivity controller. Right: the experiments with the passivity controller. At the first row, the EE positions of the master and the slave are reported. The light gray area is the rigid surface (called wall). The measured master position is in black solid line. The slave measured positions is in light gray dotted line, while the slave desired position is in dark gray dashed line. At the second row, the forces are shown: the gray dotted line is the master desired force while the black solid line is the slave measured force. At the third row, the position error between the master measured position and slave measured position is shown.

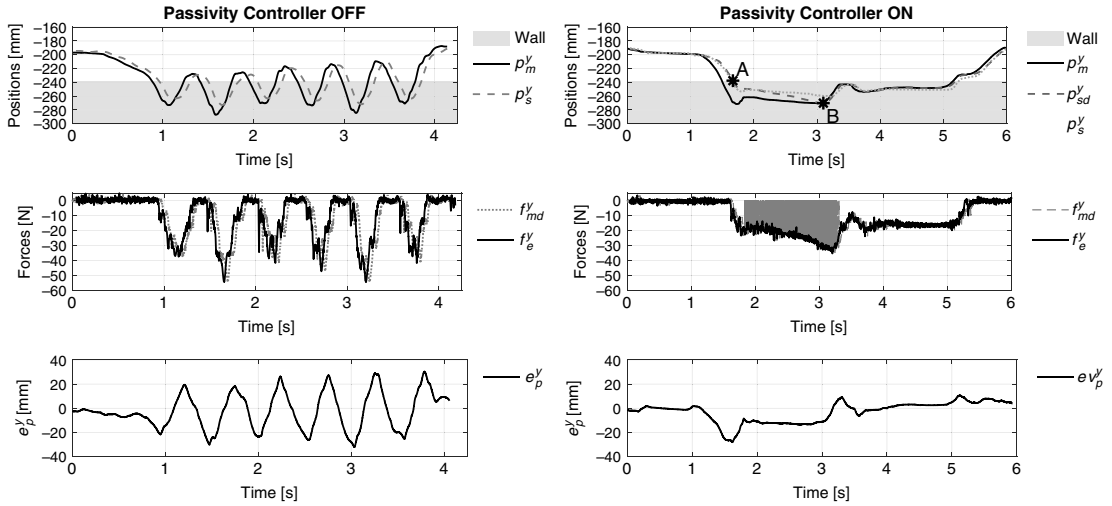

Fig. 14. Comparison between a stable and an unstable contact along the *Y*-axis. Left: the experiments without the passivity controller. Right: the experiments with the passivity controller. At the first row, the EE positions of the master and the slave are reported. The light gray area is the rigid surface (called wall). The measured master position is in black solid line. The slave measured positions is in light gray dotted line, while the slave desired position is in dark gray dashed line. At the second row, the forces are shown: the gray dotted line is the master desired force while the black solid line is the slave measured force. At the third row, the position error between the master measured position and slave measured position is shown.

4.1. Contact with stiff plate (Exp-1)

This subsection presents and discusses the results of the set of tests performed during the Exp-1. The main results of the conducted experiments are reported in the next four figures (Figs. 13–15 and 17) that share the following notation for the Cartesian space signals: p_m^x, p_m^y, p_m^z indicate the three components of the master EE position; p_s^x, p_s^y, p_s^z refer to the three components of the slave EE position; p_{sd}^x, p_{sd}^y, p_{sd}^z refer to the three components of the slave EE reference position; f_e^x, f_e^y, f_e^z indicate the three components of the interaction force between the slave EE and the environment; f_{md}^x, f_{md}^y, f_{md}^z

https://doi.org/10.1017/S0263574719000171 Published online by Cambridge University Press

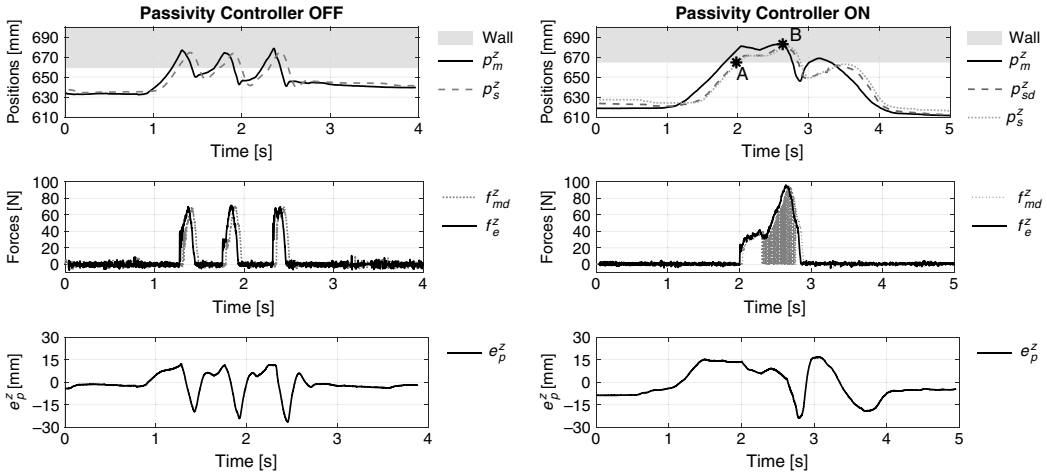

Fig. 15. Comparison between a stable and an unstable contact along the *Z*-axis. Left: the experiments without the passivity controller. Right: the experiments with the passivity controller. At the first row, the EE positions of the master and the slave are reported. The light gray area is the rigid surface (called wall). The measured master position is in black solid line. The slave measured positions is in light gray dotted line, while the slave desired position is in dark gray dashed line. At the second row, the forces are shown: the gray dotted line is the master desired force while the black solid line is the slave measured force. At the third row, the position error between the master measured position and slave measured position is shown.

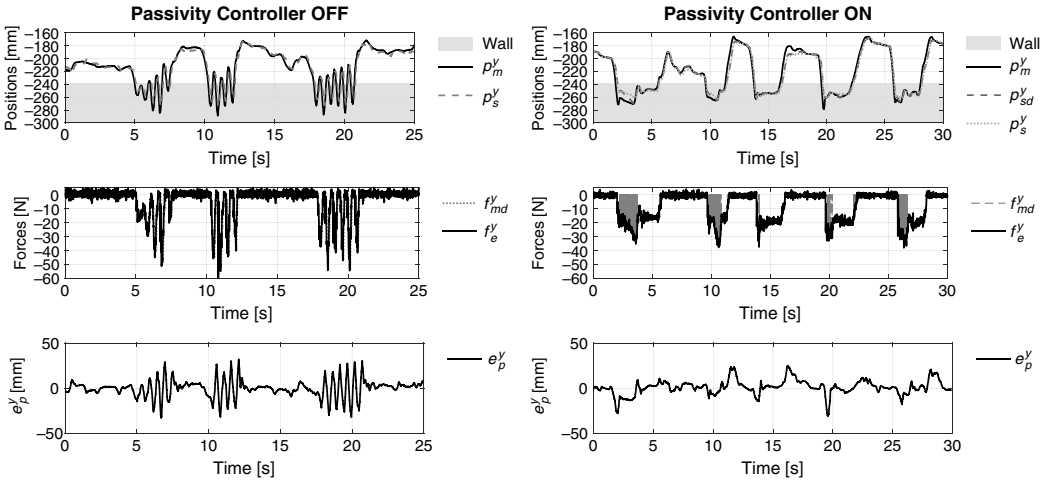

Fig. 16. Comparison between a stable and an unstable contact along the *Y*-axis. This figure shows with a different time scale (with respect to Fig. 14) the effects of the unstable contact (left) and the effects of the stable one. When the passivity controller is ON, the system remains stable and it is possible to continuously press the slave e.e. against the wall keeping a stable contact for an arbitrary amount of time.

indicate the three components of the reference force at the master EE; finally, $e_p^{x,y,z} = p_m^{x,y,z} - p_s^{x,y,z}$ are the position errors between the master and slave EE.

Figures 13–15 report the data acquired when the teleoperator system has been evaluated exerting force along only one direction at the time (*X*, *Y*, and *Z*, respectively). These figures analyze in detail a single unstable/stable contact and highlight the differences between the two cases. An example of several contacts (provided only for *Y*-axis for the sake of brevity) can be shown in Fig. 16. Focusing on the left part of the three figures that show the data acquired when the PO was OFF, it is easy to observe the unstable behavior of the whole teleoperator system. In these cases, independently of the involved axis, the subject operating with the master device has not been able to perform a stable contact with the remote stiff wall. The extra energy generation due to the communication delay causes force bursts at the master side that impede a stable contact between the slave EE and the environment. This behavior can be analyzed looking at both the oscillatory trend of master and slave position components and the force bursts at the slave side that are back propagated to the master side.

https://doi.org/10.1017/S0263574719000171 Published online by Cambridge University Press

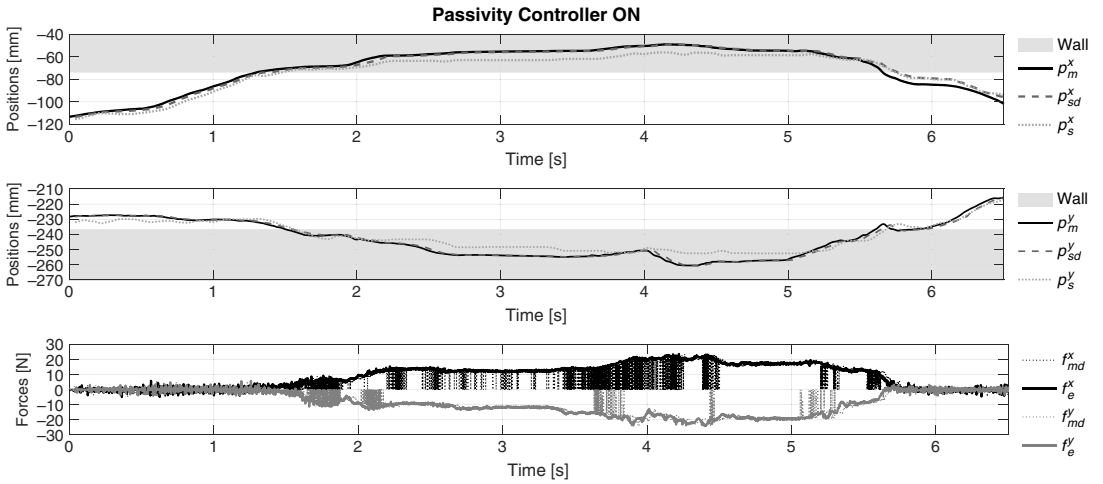

Fig. 17. The position and the force profiles along the *x*- and *y*-axes of the master and slave devices during the corner experiment with delayed communication and passivity controller enabled.

Focusing, instead, on the right part of the three figures that show the data acquired when the PO was ON, the reader can perceive the stability of the overall teleoperator system. The extra energy dissipation at the both sides, thanks to the two PCs, allows the operating subject to perform a remotely stable contact along each of the three axes. Hence, the effect is that the operator can modulate as he prefers the duration of the contact and the module of the force applied to the environment. The stability can been observed by looking at the position errors that are less jerky when the PC is enabled.

It is also worth noting that the slave position drifts with respect to the master position when the PC is enabled. In fact, it is important to remember that the position drift compensator becomes active only when the slave is not passive. As example, the reader can notice the drift during most of the *X*-axis contact duration in Fig. 13 (from point A to B), during the first contact along the *Y*-axis in Fig. 14 (from point A to B) and, in the case of the *Z*-axis, both during the contact (from point A to B). As explained above, when the slave is passive extra energy can be injected to the slave for compensating the position drift; this effect can be seen near the point B in Figs. 13–15.

As described in the experiment part, the teleoperator system has also been evaluated in multi-axes contacts. The operator was asked to push against a corner exerting hence a force having at least two main components. As example, the results of the corner experiment involving the *X*- and *Y*-axes are shown in Fig. 17. All the considerations discussed above can be applied to this practical case. The passivity controller intervenes during the contact with the corner stabilizing the interaction, avoiding a bounce effect between the two sides of the corner.

4.2. Continuous contact with a stiff surface (Exp-2)

This subsection presents the results of the experiment Exp-2 that highlight the stabilizer effect of the time-domain PC also with an asymmetrical teleoperation setup in a hard task, i.e., continuous contact where forces are exchanged over the three Cartesian axes. Figure 18(a) and 18(b) shows with a solid red line the slave robot's mean trajectories with the PC off and the PC on, respectively. This plot is a way to show in an aggregate way the position data of all the trials. The pink area around the mean is the trajectories' standard deviation for a given *x*-coordinate. A more large and spiky pink area is related with a more variable and oscillating signal. The case with the PC off exhibits a more noisy behavior and a lager standard deviation of the *x* coordinate between 200 and 280 mm respect to the PC on case.

In the mentioned range the whole teleoperation system without the passivity control started to oscillate at a relatively low frequency equal to 1.5 Hz. This behavior can be seen throw the plot in Fig. 19(a) and 19(b), respectively, for the *x*-axis and the *y*-axis. Figure 19 shows in detail the power spectral density of the slave measured forces. In a continuous contact task, the frequency spectrum of the measured forces at the slave EE provides useful information on the stability of the contact. In Fig. 19(a) and 19(b), with solid blue line the axis force when the PC off is plotted, while with a dashed red line the axis force with PC on is depicted. The plots highlight the presence of a resonance

https://doi.org/10.1017/S0263574719000171 Published online by Cambridge University Press

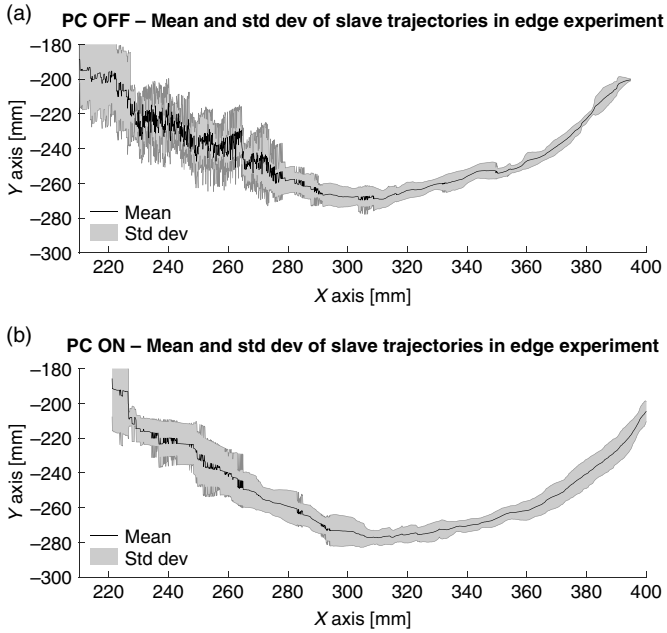

Fig. 18. Aggregates of the slave robot's end-effector positions performing the experiment Exp-2. (a) The mean trajectory when the passivity controller was off are plotted. (b) PC off case trajectory is depicted. The gray area around the mean trajectory represents the standard deviation of the *y*-coordinate for the given *x*-axis coordinate. The more the standard deviation zone is wide and spiky, the more oscillatory the slave robot is.

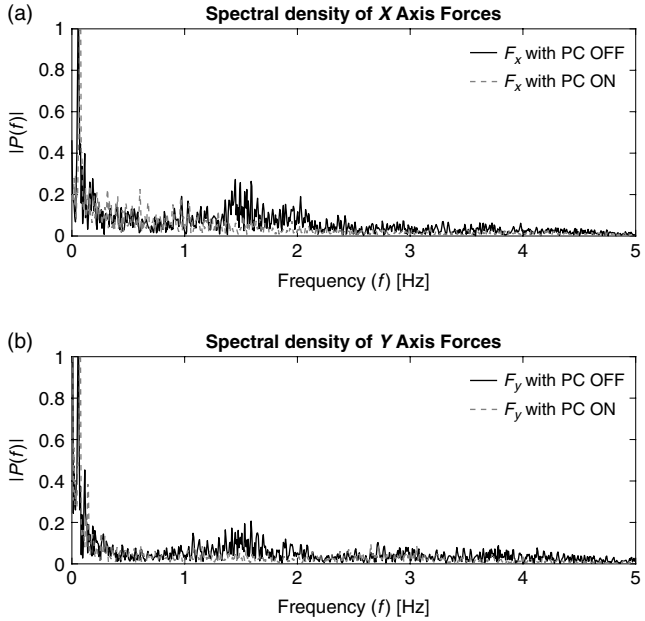

Fig. 19. The frequency spectral density of the slave's end-effector forces. With black solid line the PC off case is plotted, while with gray dashed line the PC on case is shown. (a) and (b) refer to the *x*-axis and *y*-axis forces, respectively. The PC off case spectrum exhibits a resonant frequency at 1.5 Hz the master driver was not able to compensate for.

frequency at 1.5 Hz when the delay is introduced in the communication loop and no passivity control is provided. The passivity control acts as a dissipative term: in this particular case it is in charge to dissipate the power generated at the resonant frequency.

The position and force data of a single trajectory of the edge test are provided in Fig. 20. Figure 20(a) and 20(b) shows the slave (solid blue) and the master (dashed red) robot position, respectively, in case of PC off and PC on. In the range between 200 and 280 mm of the *x*-axis the system

https://doi.org/10.1017/S0263574719000171 Published online by Cambridge University Press

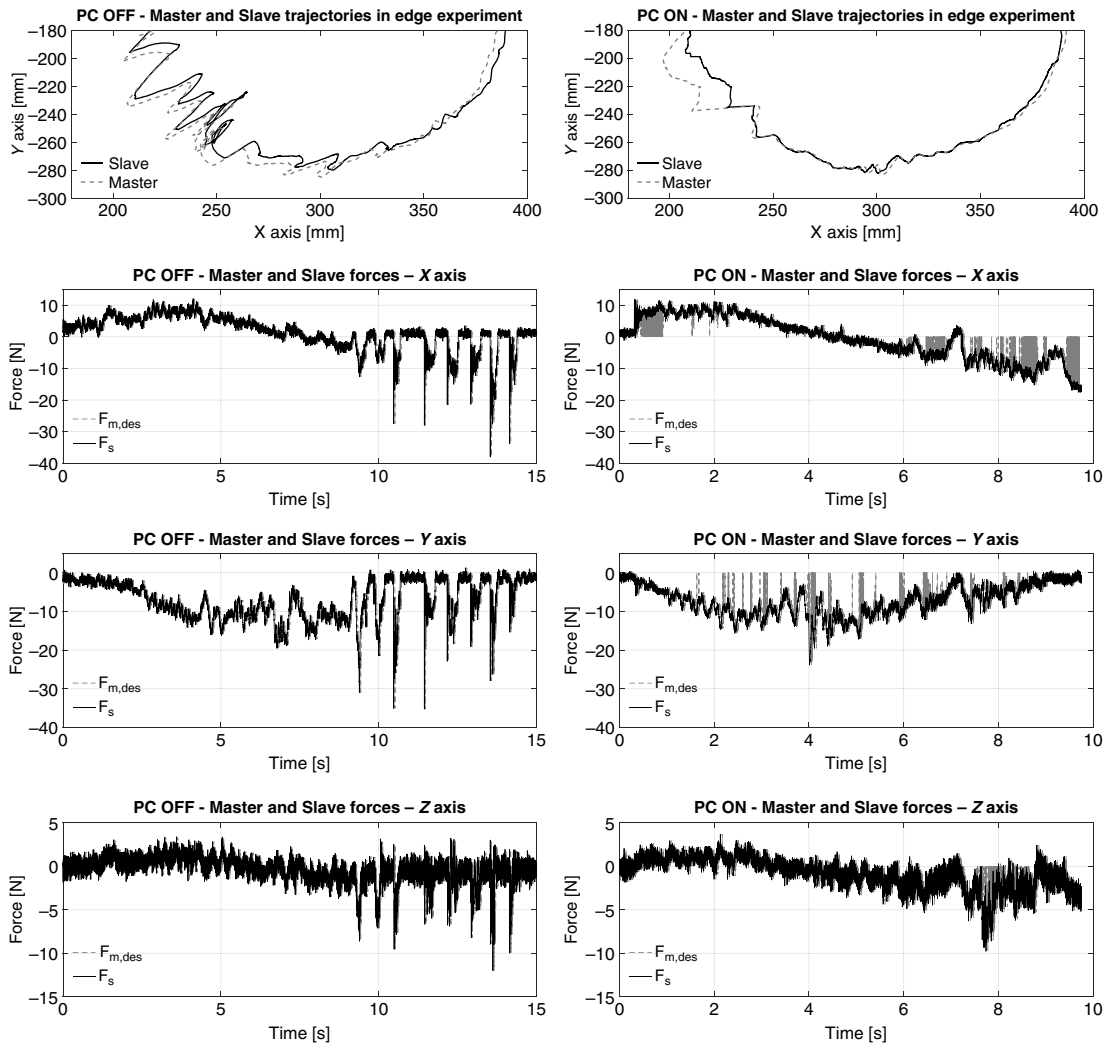

Fig. 20. The results of a single trajectory during a continuous contact with a round-shaped stiff surface. The left side is devoted to the PC off-case results, while on the right side the PC on-case results are plotted. (a, b) The slave's e.e. position (black solid) and the master's one (gray dashed). (c, h) The measured slave's e.e. forces (black solid) and the desired master's forces (gray dashed) for the three Cartesian axes. The passivity controller increases the performances in terms of smoothness of both master and slave positions; it allows to keep a stable and continuous contact by decreasing the desired master forces when the system becomes active and dissipates the energy of the unwanted oscillations.

exhibit an unstable behavior. The operator cannot stabilize the system, and this is evidenced from the forces plots in Fig. 20(c)–(e) in the time range from 8 to 15 s. In the PC off case, the slave contact forces reached values that are two times greater than the ones in the PC on case. Figure 20(f)–(h) shows how the PC dissipate the energy that is generated by the network delay through a cut of the command forces to render from the master robot. It is worth to notice that each axis contributes independently to instability and each PC acts when the related axis become active from an energetic point of view; for example in the time range from 0 to1 *s* only the *x*-axis was passivated, while in the range from 1 to 6 s only the *y*-axis was passivated and finally in the range from 6 to 9 s the three PCs acted simultaneously.

4.3. Trajectory following with a constant load at slave end-effector (Exp-3)

The experiment Exp-3 had the goal to demonstrate that the use of the PC is crucial also in the case of load carrying. The obtained results are depicted in Fig. 21 that compares the case of PC off with the PC on in the proposed task.

https://doi.org/10.1017/S0263574719000171 Published online by Cambridge University Press

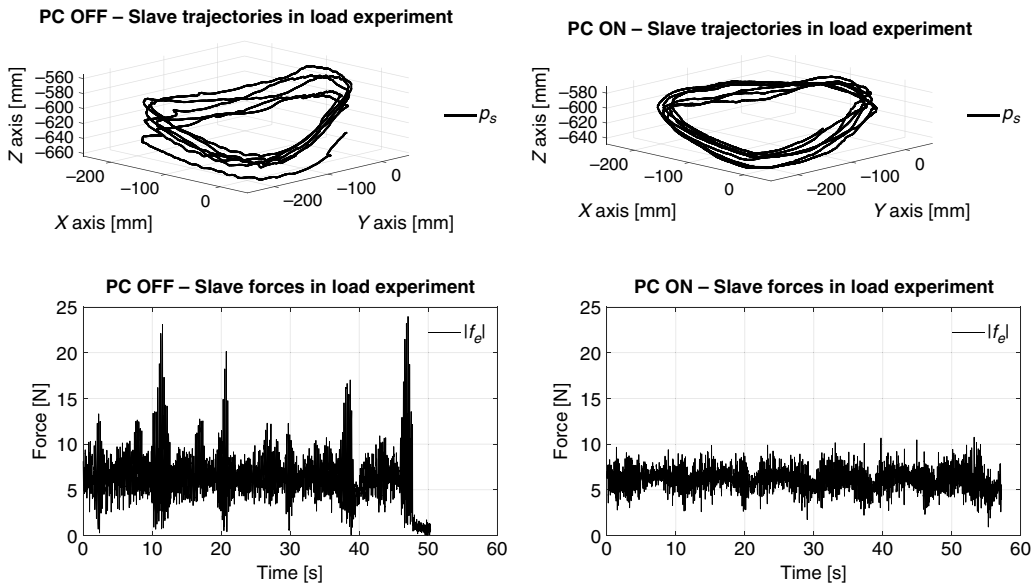

Fig. 21. The results of the experiment Exp-3 when the PC is off (left) and when the PC is on (right). Top: the measured slave's end-effector position. Bottom: the forces due to the load handling. The passivity controller is crucial also in this task; in fact, it eliminates the position oscillations and the force peaks that can be easily identified in the left side of the figure.

The load-carrying figure contains the position and force data. On top, the executed slave trajectories in the 3D space can be shown, while on the bottom part the modulus of the slave's e.e. force is plotted. The modulus of the forces was filter with a second order Butterworth low-pass filter, with a cut-off frequency of 50 Hz. The apparent noisy behavior is due to the large time scale, in fact we reported the measured forces related to all the above slave's e.e. position. Furthermore, the left side is devoted to PC off results whereas in the right side the PC on results are plotted.

The effect of the active behavior can be seen in the force signal, particularly at time $t = 10$, 20, 40, and 50 s. Moreover the modulus of the force in the case of PC off is greater than the forces in the case of PC on for the entire trajectory: the oscillations originated from the active teleoperation system generate additive inertial forces of the attached load at the EE. The PC conditions the slave's e.e. positions that result smoother and more accurate than the ones without the PC. The master exoskeleton's driver experienced an higher difficulty performing the Exp-3 in the case of PC off as highlighted from the position plot in the range from 120° to 240°.

4.4. Brief and impulsive contact with flat stiff surfaces while handling a load (Exp-4)

The experiment Exp-4 had the goal to demonstrate the ability of the TDPA to make stable a task composed of a load handling with contacts with a stiff surface. The obtained results are depicted in Fig. 22 that shows the data acquired from the teleoperator system when the PC was set on.

In detail, the overall system exhibits a stable behavior both during the load handling and the contacts with stiff surface. The results of such experiments are important since we could state that such complex teleoperator system would be able to perform several tasks that consider both load handling and stiff contacts, as example:

- to make a hole with a heavy driller;
- to use a power screw driver;
- to carry a heavy load and place it on a stiff surface.

5. Discussion

The results of the work carried out in this paper suggest that the TDPA can be successfully applied to a real complex multi-DoF teleoperation system. It is worth noting that the PCs and observers have not been directly applied at joint level (where the motors directly act) but at the EE level. This choice

https://doi.org/10.1017/S0263574719000171 Published online by Cambridge University Press

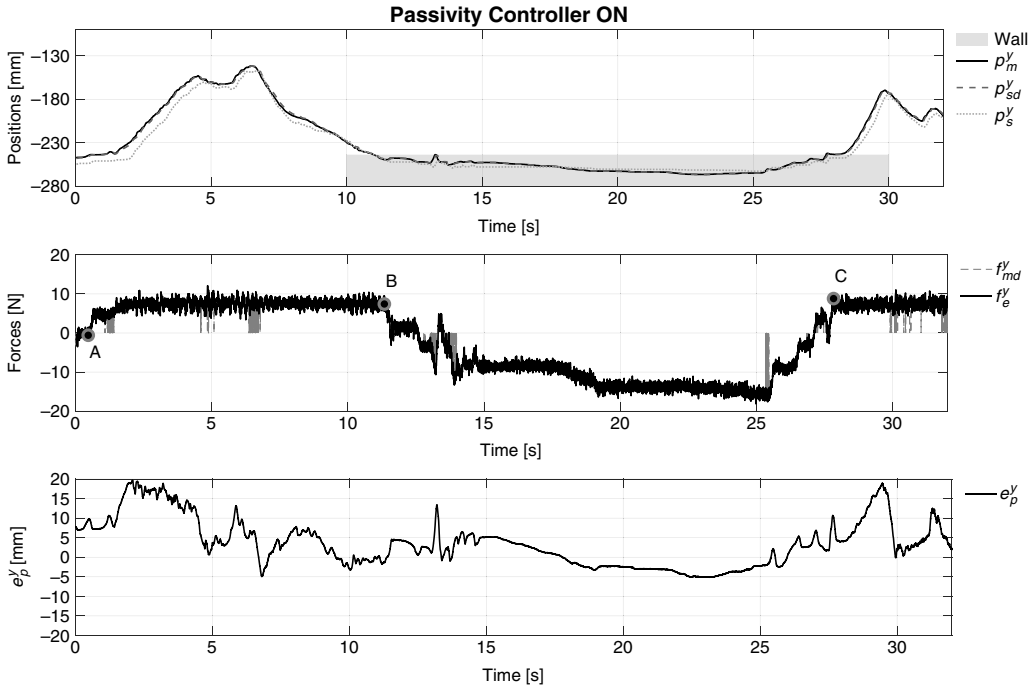

Fig. 22. The results of the experiment Exp-4 when the PC is on. Top: the measured slave's end-effector y-position. Center: the forces due to the load handling and contacts. Bottom: the position error between the slave position reference and the actual position on the y-axis. At the time point A, the load wad attached to the slave EE; the driver was asked to handle the load and perform a contact against the stiff surface. The contact begins at the time point B and lasts until the time point C.

is justified by the different link sizes of the master and slave that have the same kinematics. It turns out that the TDPA is appropriate to stabilize a system composed by an impedance-type master and admittance-type slave. This represents an important experimental validation, since such a mechanical asymmetry could be present in most teleoperation systems.

In particular, the experiments of the presented work proved the stability of the system while performing four representative tasks of particular interest in disaster-like scenarios: (1) high-force contacts against stiff wall that involve more Cartesian axes simultaneously, (2) continuous contact with a stiff edge tests, (3) heavy-load handling tests while following a predefined path, and (4) contacts against stiff surface while handling heavy load. The effectiveness of the proposed setup combined with the TDPA Position Force (measured) schema has been demonstrated also in the case of continuous contact with a stiff non-flat surface that involves the three axes simultaneously.

Despite the good results, it is worth to report that the proposed asymmetric setup presents intrinsic limitations in terms of force that can be replicated by the master due to its maximum payload and maximum stable stiffness achievable in rendering task. In fact, even though the master robot exhibits a high transparency and a low weight (that is a plus for the driver), it is not able to render high forces and very stiff environments. However, the ALEx exoskeleton has revealed to be suitable in all the tasks by using a force scaled by a factor less than one. The results have shown how the PC exhibits a larger margin of improvement in some configurations rather than others. As example, the TDPA seems to be more effective when the interaction forces are mainly along the Y-axis than the X- and Z-axes. This suggest that further studies should theoretically and quantitatively investigate the impact of the mechanical properties on the TDPA performance.

The proposed setup was tested also in the case of interaction with a purely inertial environment (Exp-3). In presence of delay, the teleoperation system started to oscillate and the presence of the attached mass leaded to an unstable behavior of the slave robot. In fact, without PC, masses with a weight greater than 1 kg could not be used to perform the test. The stabilizer effect of the PC instead leaded to a smooth interaction and allowed the handling of weights greater than 1 kg (a mass of 2.5 kg was tested and a stable behavior has been obtained).

https://doi.org/10.1017/S0263574719000171 Published online by Cambridge University Press

A critical aspect using the TDPA is the energy resetting strategy. The incorrect choice of both the reset rule or the parameter value can affect the stability of the teleoperation system. In our work we propose a strategy where the reset is activates under specific conditions such as dead time, energy levels, velocity and force levels. The choice of the parameter value has been experimentally performed, but future work might investigate an automatic procedure to adjust these parameters according to the mechanical properties of the teleoperator system.

Finally, the obtained results suggest that the proposed system with the TDPA teleoperation framework can be used as starting point to develop a more complex system. In fact, in a real scenario (as a disaster-like one), beyond 3-DoF force interaction the operator would need to perform remote dexterous object manipulation involving several DoFs.

6. Conclusions

In this experimental work, a time-domain passivity-based controller for multiple DoFs bilateral teleoperation under communication delays was implemented. The main contribution is the investigation of the application of the TDPA to a complex teleoperation system. Unlike previous related works, the presented experimental setup is composed of two isomorphic multiple DoF robots characterized by different mechanical features: the master is an impedance-type exoskeleton with good dynamic and payload characteristics, whereas the slave is a stiff and closed-loop control robot with high level of interaction forces. In this specific work, the implemented teleoperation architecture is a position–force (measured) schema with position-drift compensation. The results have shown that the TDPA is suitable to remotely control an admittance multi-DoFs robot with an admittance-type haptic interface under communication delay (80 ms round-trip). The stability has been proved by performing several (1) high-force contacts against stiff wall that involve more Cartesian axes simultaneously, (2) stiff surface following tests, (3) heavy-load handling while following a predefined path, and (4) contacts against stiff surface while handling a heavy load. The presented results suggest that the proposed system could be used as starting point for a system able to ensure more advanced robot-based remote interaction, like what is necessary either to intervene in a disaster-like scenario or to ensure a safe physiotherapist–patient interaction during a robot-based tele-rehabilitation session. Future works will focus on the analysis of a more complex teleoperator system based on a 7 DoFs upper-limb robotic exoskeleton integrating the wrist exoskeleton WRES[44] with the ALEx exoskeleton.

Acknowledgments

This work has been funded from the EU Horizon2020 project no. 644839 CENTAURO.

References

1. D. Buongiorno, M. Barsotti, E. Sotgiu, C. Loconsole, M. Solazzi, V. Bevilacqua and A. Frisoli "A Neuromusculoskeletal Model of the Human Upper Limb for a Myoelectric Exoskeleton Control Using a Reduced Number of Muscles," *2015 IEEE World Haptics Conference (WHC)* (2015) pp. 273–279. doi:10.1109/WHC.2015.7177725.
2. D. Buongiorno, F. Barone, M. Solazzi, V. Bevilacqua and A. Frisoli, "A Linear Optimization Procedure for an EMG-Driven Neuromusculoskeletal Model Parameters Adjusting: Validation Through a Myoelectric Exoskeleton Control," **In**: *Haptics: Perception, Devices, Control, and Applications* (F. Bello, H. Kajimoto and Y. Visell, eds.) (Springer International Publishing, Cham, 2016) pp. 218–227. doi:10.1007/978-3-319-42324-1_22.
3. D. Buongiorno, F. Barone, D. J. Berger, B. Cesqui, V. Bevilacqua, A. d'Avella and A. Frisoli, "Evaluation of a Pose-Shared Synergy-Based Isometric Model for Hand Force Estimation: Towards Myocontrol," **In**: *Converging Clinical and Engineering Research on Neurorehabilitation II* (J. Ibáñez, J. González-Vargas, J. M. Azorín, M. Akay and J. L. Pons, eds.) (Springer International Publishing, Cham, 2017) pp. 953–958. doi:10.1007/978-3-319-46669-9_154.
4. F. Stroppa, M. S. Stroppa, S. Marcheschi, C. Loconsole, E. Sotgiu, M. Solazzi, D. Buongiorno and A. Frisoli, "Real-Time 3D Tracker in Robot-Based Neurorehabilitation," **In**: *Computer Vision for Assistive Healthcare. Computer Vision and Pattern Recognition* (M. Leo and G. M. Farinella, eds.), Chapter 3 (Academic Press, 2018) pp. 75–104. doi:10.1016/B978-0-12-813445-0.00003-4.
5. D. Buongiorno, M. Barsotti, F. Barone, V. Bevilacqua and A. Frisoli, "A linear approach to optimize an EMG-driven neuromusculoskeletal model for movement intention detection in myo-control: A case study on shoulder and elbow joints," *Front. Neurorob.* **12**, 74 (2018). doi:10.3389/fnbot.2018.00074.
6. D. Chiaradia, M. Xiloyannis, C. W. Antuvan, A. Frisoli and L. Masia, "Design and Embedded Control of a Soft Elbow Exosuit," *Proceedings of IEEE International Conference on Soft Robotics (RoboSoft), Livorno, Italy* (IEEE, 2018). doi:10.1109/ROBOSOFT.2018.8405386.

7. D. Chiaradia, M. Xiloyannis, M. Solazzi, L. Masia and A. Frisoli, "Comparison of a Soft Exosuit and a Rigid Exoskeleton in an Assistive Task," **In**: *Wearable Robotics: Challenges and Trends* (M. C. Carrozza, S. Micera and J. L. Pons, eds.) (Springer International Publishing, Cham, 2019) pp. 415–419. doi:10.1007/978-3-030-01887-0_80.
8. M. Xiloyannis, L. Galli, D. Chiaradia, A. Frisoli, F. Braghin and L. Masia, "A Soft Tendon-Driven Robotic Glove: Preliminary Evaluation," **In**: *Converging Clinical and Engineering Research on Neurorehabilitation III* (L. Masia, S. Micera, M. Akay and J. L. Pons, eds.) (Springer International Publishing, Cham, 2019) pp. 329–333. doi:10.1007/978-3-030-01845-0_66.
9. M. Xiloyannis, D. Chiaradia, A. Frisoli and L. Masia, "Characterisation of Pressure Distribution at the Interface of a Soft Exosuit: Towards a More Comfortable Wear," **In**: *Wearable Robotics: Challenges and Trends* (M. C. Carrozza, S. Micera and J. L. Pons, eds.) (Springer International Publishing, Cham, 2019) pp. 35–38. doi:10.1007/978-3-030-01887-0_7.
10. D. J. Reinkensmeyer, C. T. Pang, J. A. Nessler and C. C. Painter, "Web-based telerehabilitation for the upper extremity after stroke," *IEEE Trans. Neural Syst. Rehabil. Eng.* **10**(2), 102–108 (2002).
11. C. R. Carignan and H. I. Krebs, "Telerehabilitation robotics: Bright lights, big future?" *J. Rehabil. Res. Dev.* **43**(5), 695 (2006).
12. K. D. Katyal, C. Y. Brown, S. A. Hechtman, M. P. Para, T. G. McGee, K. C. Wolfe, R. J. Murphy, M. D. Kutzer, E. W. Tunstel, M. P. McLoughlin and M. S. Johannes, "Approaches to Robotic Teleoperation in a Disaster Scenario: From Supervised Autonomy to Direct Control," *2014 IEEE/RSJ International Conference on Intelligent Robots and Systems (IROS 2014)*, Chicago, IL, USA (IEEE, 2014) pp. 1874–1881.
13. H. Martins and R. Ventura "Immersive 3-D Teleoperation of a Search and Rescue Robot Using a Head-Mounted Display," *IEEE Conference on Emerging Technologies & Factory Automation, 2009. ETFA 2009*, Mallorca, Spain (IEEE, 2009), pp. 1–8.
14. R. Cisneros, S. Kajita, T. Sakaguchi, S. Nakaoka, M. Morisawa, K. Kaneko and F. Kanehiro, "Task-Level Teleoperated Manipulation for the HRP-2Kai Humanoid Robot," *2015 IEEE-RAS 15th International Conference on Humanoid Robots (Humanoids)*, Seoul, South Korea (IEEE, 2015) pp. 1102–1108.
15. D. Lawrence, "Stability and transparency in bilateral teleoperation," *IEEE Trans. Rob. Autom.* **9**(5), 624–637 (1993).
16. L. Chan, F. Naghdy and D. Stirling, "Application of adaptive controllers in teleoperation systems: A survey," *IEEE Trans. Hum.-Mach. Syst.* **44**(3), 337–352 (2014).
17. P. F. Hokayem and M. W. Spong, "Bilateral teleoperation: An historical survey," *Automatica* **42**(12), 2035–2057 (2006).
18. R. Anderson and M. Spong, "Asymptotic stability for force reflecting teleoperators with time delays," *1989 IEEE International Conference on Robotics and Automation, 1989. Proceedings*, Scottsdale, AZ, USA (IEEE, 1989) pp. 1618–1625.
19. G. Niemeyer and J. J. Slotine, "Stable adaptive teleoperation," *IEEE J. Oceanic Eng.* **16**(1), 152–162 (1991).
20. D. A. Lawrence, "Stability and transparency in bilateral teleoperation," *Proceedings of the 31st IEEE Conference on Decision and Control, 1992*, Tucson, AZ, USA (IEEE, 1992) pp. 2649–2655.
21. P. Buttolo, P. Braathen and B. Hannaford, "Sliding control of force reflecting teleoperation: Preliminary studies," *Presence: Teleoperators Virtual Environ.* **3**(2), 158–172 (1994).
22. G. M. Leung, B. A. Francis and J. Apkarian, "Bilateral controller for teleoperators with time delay via μ-synthesis," *IEEE Trans. Rob. Autom.* **11**(1), 105–116 (1995).
23. P. Mitra and G. Niemeyer, "Model-mediated telemanipulation," *Int. J. Rob. Res.* **27**(2), 253–262 (2008).
24. M. Schwarz, T. Rodehutskors, D. Droeschel, M. Beul, M. Schreiber, N. Araslanov, I. Ivanov, C. Lenz, J. Razlaw, S. Schüller, D. Schwarz, A. Topalidou-Kyniazopoulou and S. Behnke, "Nimbro rescue: Solving disaster-response tasks with the mobile manipulation robot momaro," *J. Field Rob.* **34**(2), 400–425 (2017).
25. A. Ajoudani, J. Lee, A. Rocchi, M. Ferrati, E. M. Hoffman, A. Settimi, D. G. Caldwell, A. Bicchi and N. G. Tsagarakis, "A Manipulation Framework for Compliant Humanoid Coman: Application to a Valve Turning Task," *2014 14th IEEE-RAS International Conference on Humanoid Robots (Humanoids)*, Madrid, Spain (IEEE, 2014) pp. 664–670.
26. Y. S. Kim, J. Lee, S. Lee and M. Kim, "A force reflected exoskeleton-type masterarm for human-robot interaction," *IEEE Tran. Syst. Man Cybern. Part A: Syst. Hum.* **35**(2), 198–212 (2005).
27. E. Pirondini, M. Coscia, S. Marcheschi, G. Roas, F. Salsedo, A. Frisoli, M. Bergamasco and S. Micera, "Evaluation of a New Exoskeleton for Upper Limb Post-stroke Neuro-rehabilitation: Preliminary Results," **In**: *Replace, Repair, Restore, Relieve–Bridging Clinical and Engineering Solutions in Neurorehabilitation* (Springer, Aalborg, 2014) pp. 637–645.
28. S. F. Atashzar, M. Shahbazi, M. Tavakoli and R. V. Patel, "A passivity-based approach for stable patient–robot interaction in haptics-enabled rehabilitation systems: Modulated time-domain passivity control," *IEEE Trans. Control Syst. Technol.* **25**(3), 991–1006 (2017).
29. J. Artigas, R. Balachandran, C. Riecke, M. Stelzer, B. Weber, J. H. Ryu and A. Albu-Schaeffer, "KONTUR-2: Force-Feedback Teleoperation from the International Space Station," *2016 IEEE International Conference on Robotics and Automation (ICRA)*, Stockholm, Sweden (IEEE, 2016) pp. 1166–1173.
30. V. Chawda and M. K. O'Malley, "Position synchronization in bilateral teleoperation under time-varying communication delays," *IEEE/ASME Trans. Mechatron.* **20**(1), 245–253 (2015).

31. B. Han, J. H. Ryu and I. K. Jung, "FPGA Based Time Domain Passivity Observer and Passivity Controller," *IEEE/ASME International Conference on Advanced Intelligent Mechatronics, 2009. AIM 2009*, Singapore (IEEE, 2009) pp. 433–438.
32. V. Chawda, H. Van Quang, M. K. O'Malley and J. H. Ryu, "Compensating Position Drift in Time Domain Passivity Approach Based Teleoperation," *2014 IEEE Haptics Symposium (HAPTICS)*, Houston, TX, USA (IEEE, 2014) pp. 195–202.
33. J. Artigas, J. H. Ryu and C. Preusche, "Time domain passivity control for position-position teleoperation architectures," *Presence* **19**(5), 482–497 (2010).
34. E. Pirondini, M. Coscia, S. Marcheschi, G. Roas, F. Salsedo, A. Frisoli, M. Bergamasco and S. Micera, "Evaluation of the effects of the arm light exoskeleton on movement execution and muscle activities: a pilot study on healthy subjects," *J. Neuroeng. Rehabil.* **13**(1), 9 (2016).
35. R. Vertechy, A. Frisoli, A. Dettori, M. Solazzi and M. Bergamasco, "Development of a New Exoskeleton for Upper Limb Rehabilitation," *IEEE International Conference on Rehabilitation Robotics, 2009. ICORR 2009*, Kyoto, Japan (IEEE, 2009) pp. 188–193.
36. M. Solazzi, M. Abbrescia, R. Vertechy, C. Loconsole, V. Bevilacqua and A. Frisoli, "An Interaction Torque Control Improving Human Force Estimation of the Rehab-Exos Exoskeleton," *2014 IEEE Haptics Symposium (HAPTICS)*, Houston, TX, USA (IEEE, 2014) pp. 187–193.
37. B. Hannaford and J. H. Ryu, "Time-domain passivity control of haptic interfaces," *IEEE Trans. Rob. Autom.* **18**(1), 1–10 (2002).
38. J. H. Ryu, D. S. Kwon and B. Hannaford, 'Stable teleoperation with time-domain passivity control', *IEEE Trans. Rob. Autom.* **20**(2), 365–373 (2004).
39. M. Panzirsch, T. Hulin, J. Artigas, C. Ott and M. Ferre, "Integrating Measured Force Feedback in Passive Multilateral Teleoperation," *International Conference on Human Haptic Sensing and Touch Enabled Computer Applications*, London, UK (Springer, 2016) pp. 316–326.
40. J. Artigas, J. H. Ryu, C. Preusche and G. Hirzinger, "Network Representation and Passivity of Delayed Teleoperation Systems," *2011 IEEE/RSJ International Conference on Intelligent Robots and Systems*, San Francisco, CA, USA (IEEE, 2011) pp. 177–183.
41. Y. S. Kim and B. Hannaford, "Some Practical Issues in Time Domain Passivity Control of Haptic Interfaces," *2001 IEEE/RSJ International Conference on Intelligent Robots and Systems, 2001. Proceedings*, Maui, HI, USA, vol. 3 (IEEE, 2001) pp. 1744–1750.
42. J. H. Ryu, 'Bilateral Control with Time Domain Passivity Approach Under Time-Varying Communication Delay," *The 16th IEEE International Symposium on Robot and Human Interactive Communication, 2007. RO-MAN 2007*, Jeju, South Korea (IEEE, 2007) pp. 986–991.
43. L. Sciavicco and B. Siciliano, *Modelling and Control of Robot Manipulators* (Springer Science & Business Media, London, UK, 2012)
44. D. Buongiorno, E. Sotgiu, D. Leonardis, S. Marcheschi, M. Solazzi and A. Frisoli, "WRES: A novel 3 DoF wrist exoskeleton with tendon-driven differential transmission for neuro-rehabilitation and teleoperation," *IEEE Rob. Autom. Lett.* **3**(3), 2152–2159 (2018). doi:10.1109/LRA.2018.2810943.

Appendix: Definition of the communication network energies and the passivity observers

A.1. Definition of the communication network energies

The discrete expressions of energy flows traveling through the two TDPNs $E_{N_a}(t)$ and $E_{N_b}(t)$ can be written as follows:

$$\begin{aligned} E_{N_a}(n) &= \Delta T \sum_{k=0}^{k=n} \left[f_e(k - T_b) v_m(k) - f_e(k) v_m(k - T_f) \right] \\ E_{N_b}(n) &= \Delta T \sum_{k=0}^{k=n} \left[f_s(k - T_b) v_m(k) - f_s(k) v_m(k - T_f) \right] \end{aligned} \tag{A1}$$

where ΔT is the sampling time. The Expression of the flows N_a and N_b depends on the sources E_{C_a} and E_{C_b} that are as follows:

$$\begin{aligned} E_{C_a}(n) &= \Delta T \sum_{k=0}^{k=n} -f_e(k) v_m(k - T_f) \\ E_{C_b}(n) &= \Delta T \sum_{k=0}^{k=n} f_s(k - T_b) v_m(k) \end{aligned} \tag{A2}$$

https://doi.org/10.1017/S0263574719000171 Published online by Cambridge University Press

A.2. Definition of the passivity observers

Following,[40] the equations of the two POs, $W_S(n)$ and $W_M(n)$, for each port of the network are given as follows:

$$\begin{aligned} W_S(n) &= \frac{1}{\Delta T}\left[E_{in}^{Mb}(n-T_{kf}) - E_{out}^{Sb}(n) + E_{BPC}^{S}(n-1)\right] \\ E_{in}^{Mb}(n) &= \Delta T \sum_{n=0}^{n=k} f_s(n-T_{kb})v_m(n) \\ &\quad \textbf{if} \quad f_s(n-T_{kb})v_m(n) > 0 \\ E_{out}^{Sb}(n) &= \Delta T \sum_{n=0}^{n=k} -f_s(n)v_m(n-T_{kf}) \\ &\quad \textbf{if} \quad f_s(n)v_m(n-T_{kf}) < 0 \end{aligned} \tag{A3}$$

$$\begin{aligned} W_M(n) &= \frac{1}{\Delta T}\left[E_{in}^{Sa}(n-T_{kb}) - E_{out}^{Ma}(n) + E_{FPC}^{M}(n-1)\right] \\ E_{in}^{Sa}(n) &= \Delta T \sum_{n=0}^{n=k} f_e(n)v_m(n-T_{kf}) \\ &\quad \textbf{if} \quad f_e(n)v_m(n-T_{kf}) > 0 \\ E_{out}^{Ma}(n) &= \Delta T \sum_{n=0}^{n=k} -f_e(n-T_{kb})v_m(n) \\ &\quad \textbf{if} \quad f_e(n-T_{kb})v_m(n) < 0 \end{aligned} \tag{A4}$$

https://doi.org/10.1017/S0263574719000171 Published online by Cambridge University Press